

# Journal Pre-proof

Morphological and ultrastructural alterations of zebrafish (*Danio rerio*) spermatozoa after motility activation

Paula Sáez-Espinosa, Cristina Franco-Esclapez, Laura Robles-Gómez, Willian T.A.F. Silva, Alejandro Romero, Simone Immler, María José Gómez-Torres



PII: S0093-691X(22)00206-0

DOI: <https://doi.org/10.1016/j.theriogenology.2022.05.025>

Reference: THE 16297

To appear in: *Theriogenology*

Received Date: 13 January 2022

Revised Date: 24 May 2022

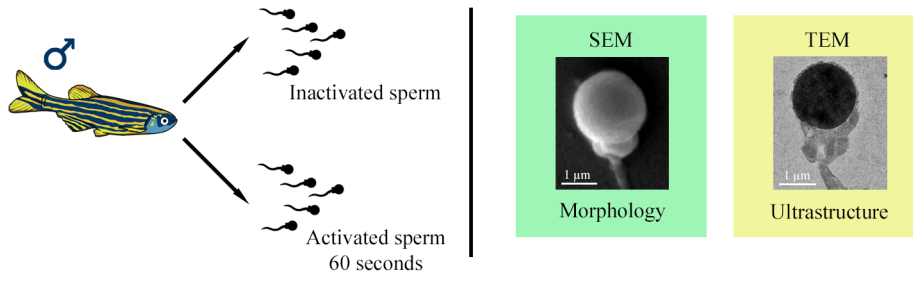
Accepted Date: 28 May 2022

Please cite this article as: Sáez-Espinosa P, Franco-Esclapez C, Robles-Gómez L, Silva WTAF, Romero A, Immler S, Gómez-Torres MaríJosé, Morphological and ultrastructural alterations of zebrafish (*Danio rerio*) spermatozoa after motility activation, *Theriogenology* (2022), doi: <https://doi.org/10.1016/j.theriogenology.2022.05.025>.

This is a PDF file of an article that has undergone enhancements after acceptance, such as the addition of a cover page and metadata, and formatting for readability, but it is not yet the definitive version of record. This version will undergo additional copyediting, typesetting and review before it is published in its final form, but we are providing this version to give early visibility of the article. Please note that, during the production process, errors may be discovered which could affect the content, and all legal disclaimers that apply to the journal pertain.

© 2022 Published by Elsevier Inc.

**Morphological and ultrastructural alterations of zebrafish (*Danio rerio*) spermatozoa after motility activation**



Journal Pre-proof

1 **Morphological and ultrastructural alterations of zebrafish (*Danio rerio*)**  
2 **spermatozoa after motility activation**

3 Paula Sáez-Espinosa<sup>a</sup>; Cristina Franco-Esclapez<sup>a</sup>; Laura Robles-Gómez<sup>a</sup>; Willian T. A.  
4 F. Silva<sup>b</sup>; Alejandro Romero<sup>a</sup>; Simone Immler<sup>c</sup>; María José Gómez-Torres<sup>a,d,\*</sup>

5

6 <sup>a</sup> Departamento de Biotecnología, Universidad de Alicante, Alicante, Spain.

7 <sup>b</sup> Centre for Environmental and Climate Science, Lund University, Lund, Sweden.

8 <sup>c</sup> School of Biological Sciences, University of East Anglia, Norwich, UK.

9 <sup>d</sup> Cátedra Human Fertility, Universidad de Alicante, Alicante, Spain.

10

11 \*Corresponding author:

12 María José Gómez-Torres

13 Departamento de Biotecnología, Universidad de Alicante, 03080, Alicante, Spain.

14 Tlf: +34 965903878; e-mail: mjose.gomez@ua.es

15 **Abstract**

16 Spermatozoa motility in freshwater and marine fish is mainly controlled by the difference  
17 in osmotic pressure. Specifically, zebrafish (*Danio rerio*) spermatozoa undergo  
18 hypoosmotic shock due to the decrease in extracellular potassium, which leads to  
19 membrane hyperpolarization and activation of flagellar motility. Previous studies have  
20 concluded that motility activation has a negative effect on the spermatozoa structure.  
21 However, no evidence exists about ultrastructural changes in zebrafish spermatozoa after  
22 motility activation. In this study, spermatozoa samples were obtained from ten adult  
23 zebrafish individuals before and 60 seconds after motility activation and analyzed using  
24 Scanning and Transmission Electron Microscopy. Results showed dramatic  
25 morphological and ultrastructural alterations of the zebrafish spermatozoa after  
26 activation. In particular, the spermatozoa head underwent severe morphological  
27 distortion, including swelling of the nucleus, the bursting of the plasma membrane, and  
28 the alteration of the genetic material. Midpieces were also affected after activation since  
29 rupture of the cell membrane and lysis of mitochondria occurred. Furthermore, after the  
30 hypoosmotic shock, most spermatozoa showed a coiled flagellum and a disaggregated  
31 plasma membrane. Overall, our findings show that the activation of motility leads to  
32 substantial zebrafish spermatozoa morphological and ultrastructural changes, which  
33 could modify their physiology and decrease the fertilizing potential.

34

35 **Key words:** motility activation, sperm morphology, ultrastructure microscopy, zebrafish.

## 36 1. Introduction

37 The zebrafish (*Danio rerio*, cyprinid, teleost) is a freshwater fish which has become a  
38 potential biomedical model [1,2]. Particularly, in reproductive and developmental  
39 physiology, the zebrafish is widely used due to their high fertilization rate, short  
40 reproductive cycle, and rapid embryo development [3]. In addition, fertilization in  
41 zebrafish is external and eggs, embryos and early larvae are transparent, a special  
42 characteristic that facilitates the study of their ontogenetic development [4,5].

43 External fertilization implies particular spermatozoa physiological traits, such as  
44 the activation of flagellar motility when they come into contact with freshwater and the  
45 increase of intracellular pH altered by internal ionic concentration [6–9]. Specifically,  
46 zebrafish spermatozoa undergo hypoosmotic shock due to depletion of extracellular  
47 potassium. This scenario leads to the activation of cyclic nucleotide-operated potassium  
48 cation channels (CNGK), resulting in hyperpolarization of the membrane that leads to the  
49 opening of voltage-gated calcium channels (Cav) [10]. Furthermore, the increase in  
50 intracellular calcium activates flagellar motility in an optimal activation range between  
51 150 and 210 mosmol Kg<sup>-1</sup> [11].

52 Moreover, the duration of spermatozoa motility is shorter in freshwater fish than  
53 marine fish due to limiting factors such as low resistance to hypoosmotic shock and  
54 increased calcium concentration [12]. It is important to highlight that the disposition of  
55 energy in the form of Adenosine triphosphate (ATP) is not a limiting factor, as shown by  
56 the presence of intracellular ATP even after the arrest of movement [13,14]. Therefore,  
57 the spermatozoa structural damage caused by the hypoosmotic shock is the main limiting  
58 factor to the duration of motility in freshwater fish [12], which show up to a maximum of  
59 120 seconds of active motility in some teleost species [15]. The duration of motility in

60 zebrafish spermatozoa is 60 seconds at absolute maximum, during which spermatozoa  
61 must reach and fertilize the oocyte [16,17].

62 Mitochondrial ATP stores are essential for the initiation and maintenance of  
63 spermatozoa motility. In this context, spermatozoa mitochondria have morphological  
64 differences depending on the species. For instance, they are usually oval in most  
65 mammalian, while in fish they can be cylindrical, irregular, or spherical, as in the case of  
66 zebrafish [18]. Likely, the mitochondria size and number depend on the energy demand  
67 of each specie. Nevertheless, a strong connection between the number or arrangement of  
68 mitochondria and spermatozoa motility, duration, and speed has not yet been determined  
69 [19].

70 Changes in spermatozoa morphology and ultrastructure after activation have been  
71 studied in fish species such as the common carp (*Cyprinus carpio*) [14], sea bass  
72 (*Dicentrarchus labrax*) [13], and northern pike (*Esox lucius*) [6]. Overall, these studies  
73 revealed several marked morphological inter-specific changes such as the alteration of  
74 the plasma membrane, the swelling of the head, and the coiling of the flagellum.  
75 However, the morphological and ultrastructural changes that occur in zebrafish  
76 spermatozoa after the motility activation remains to be elucidated. Given the potential of  
77 zebrafish as a biomedical model in developmental biology, the aim of this study was to  
78 characterize by means of Scanning Electron Microscopy (SEM) and Transmission  
79 Electron Microscopy (TEM) the morphological and ultrastructural changes in zebrafish  
80 sperm after motility activation.

## 81 2. Materials and methods

### 82 2.1. Sample collection and experimental design

83 We collected zebrafish spermatozoa from the AB wild-type strain obtained from  
84 Zebrafish International Resource Center (ZIRC) and bred under an outbreeding regime at

85 the SciLifeLab zebrafish facility at Uppsala University (Sweden). The fish were raised to  
86 sexual maturity and kept under standard laboratory conditions at a temperature of 28°C,  
87 a 12/12-hour light/dark cycle, and an *ad libitum* feeding regime with live *Artemia* (ZM  
88 Systems, UK) and dry food (Medium granular, ZM Systems, UK) three (adult) to five  
89 (juvenile) times a day following previous protocols [20]. The experimental protocols were  
90 approved by the Swedish Board of Agriculture (Jordbruksverket, approval no. C 3/15).

91 Spermatozoa were collected from ten adult males placed in 10L tank containing  
92 approximately 50 fish/tank and a sex ratio of approximately 1:1. For spermatozoa  
93 collection, males were first anesthetized in a 0.016% (*w/v*) tricaine methanesulfonate  
94 (MS-222) solution (Sigma-Aldrich®, St. Louis, MO, USA) for a maximum of two  
95 minutes, briefly rinsed in system water and placed ventral side up into a moist sponge  
96 under a stereomicroscope. A paper towel was used to blot dry the genital pore and avoid  
97 unwanted spermatozoa activation upon contact with water. Using a calibrated micro-  
98 capillary (Sigma-Aldrich®), spermatozoa were collected, immediately mixed with 50 µL  
99 of Hank's buffer in microtubes, recipe described in [21], and placed on ice until further  
100 steps were conducted.

101 Each ejaculate was split into two subsamples to obtain the two experimental  
102 conditions: inactivated spermatozoa (IS) and activated spermatozoa (AS) after 60 seconds  
103 of tap water activation (Fig 1A). This time was chosen because the duration of zebrafish  
104 motility is approximately 60 seconds [16,17]. Spermatozoa from both different  
105 experimental conditions (IS and AS) were fixed to analyze the detailed morphology and  
106 the ultrastructure of zebrafish spermatozoa by using SEM and TEM, respectively (Fig  
107 1B). Cells were fixed in 2% (*v/v*) glutaraldehyde (one volume of spermatozoa in Hank's  
108 buffer and water to one volume of 4% (*v/v*) glutaraldehyde). After one hour of fixation at  
109 4°C, cells were centrifuged (350 g, five minutes) to replace glutaraldehyde with

110 phosphate-buffered saline without calcium or magnesium, pH 7.4 (PBS, Biowest,  
111 Nuaille, France). The final sperm concentration was adjusted around  $10 \times 10^6/\text{ml}$  and  
112 conserved at  $4^\circ\text{C}$  until use.

### 113 *2.2.Spermatozoa morphological analysis*

114 After the primary fixation, a total of  $5 \mu\text{l}$  of spermatozoa sample was then placed on a  
115 glass coverslip and dehydrated in an increasing ethanol series and critical point dried in  
116 carbon dioxide (EMS850, Electron Microscopy Sciences, Hatfield, PA, USA). All  
117 coverslips were glued to the stubs by carbon adhesive tape, then gold sputtered (Balzers  
118 SCD 004 Sputter Coater) and examined using a Scanning Electron Microscope (SEM)  
119 Hitachi S3000N (Hitachi Ltd., Tokyo, Japan). High-resolution SEM micrographs of  
120 spermatozoa were recorded at standardized  $\times 4,000$  magnification and an accelerating  
121 voltage of 15 kV from each experimental group (IS and AS). Around 100 random IS and  
122 AS zebrafish spermatozoa SEM micrographs were captured.

### 123 *2.3.Spermatozoa ultrastructural analysis*

124 The fixed-glutaraldehyde spermatozoa were embedded in small blocks of 2% ( $w/v$ ) agar  
125 (Sigma-Aldrich<sup>®</sup>) and allowed to solidify at  $4^\circ\text{C}$  overnight. Then, samples were post-  
126 fixed with 1% osmium tetroxide (Electron Microscopy Sciences) and washed three times  
127 with PBS. At that point, the spermatozoa blocks were dehydrated in an ascending series  
128 of ethanol concentrations and embedded in epoxy resin EPON-812 (Electron Microscopy  
129 Sciences). Ultrathin spermatozoa sections were obtained using an ultramicrotome Leica  
130 Ultracut R (Leica, Wetzlar, Germany) with a diamond knife and deposited on a copper  
131 grid. Later, ultrathin sections were double contrasted by 5% ( $v/v$ ) uranyl acetate and 2.5%  
132 ( $v/v$ ) lead citrate. Finally, that spermatozoa section were examined using a Transmission  
133 Electron Microscope (TEM) JEOL JEM-1400 Plus (JEOL Ltd., Tokyo, Japan) equipped  
134 with a Gatan Orius digital camera (Gatan, Pleasanton, CA, USA) for capturing

135 micrographs. Around 100 random IS and AS zebrafish spermatozoa TEM micrographs  
136 were captured.

#### 137 *2.4. Metric and statistical analyses*

138 The length and width of the head, nucleus, midpiece, and flagellum were measured in  
139 micrometers ( $\mu\text{m}$ ) from 70-105 random SEM micrographs of IS and AS zebrafish  
140 spermatozoa. In addition, a total of 50 mitochondria TEM micrographs were used to  
141 analyze the nanometric (nm) size-related mitochondrial morphology from both IS and AS  
142 conditions. Head, nucleus, and mitochondrial area were also recorded. Measurements  
143 were conducted using ImageJ (U. S. National Institutes of Health). Unpaired two-sample  
144 *t*-test was conducted to determine the source of significant metric variation among IS and  
145 AS conditions according to Levene's test for equality of variances. Descriptive (mean  $\pm$   
146 SD; standard deviation) statistics were reported and test statistics at  $\alpha = 0.05$  significance  
147 level were performed using IBM® SPSS® Statistics v. 21.0 (IBM, Armonk, NY, USA).

### 148 **3. Results**

#### 149 *3.1. Morphological and ultrastructural description of IS*

150 SEM analysis allowed differentiating the structure of *Danio rerio* mature spermatozoa  
151 (Fig 2A). The morphology consisted of a spherical head without acrosome (Fig 2B), a  
152 short intermediate midpiece, and a flagellum that comes out through the midpiece and  
153 ends in a terminal piece. The mean total length  $\pm$  SD of the sperm was  $31.94 \pm 2.01 \mu\text{m}$ ,  
154 dividing into  $1.83 \pm 0.12 \mu\text{m}$  of head,  $0.59 \pm 0.13 \mu\text{m}$  of midpiece, and  $28.74 \pm 2.14 \mu\text{m}$   
155 of flagellum (Table 1).

156 In addition, zebrafish IS ultrastructure registered by TEM (Fig 3A-F) showed a  
157 spherical head without acrosome presence. The cephalic region was completely occupied  
158 by the nucleus with a compacted homogeneous chromatin, although small nuclear  
159 vacuoles with lower density were also observed (Fig 3E). The nuclear area was obtained

160 from TEM micrographs and results registered a mean of  $2.03 \pm 0.36 \mu\text{m}^2$  (Table 1).  
161 Furthermore, the nucleus was delimited by a nuclear membrane, which in turn was  
162 surrounded by a plasma membrane (Fig 3D,E), encompassing the rest of the structures.  
163 In addition, the presence of a nuclear fossa was noted (Fig 3E) as a depression in the  
164 lower surface of the nucleus where the proximal centriole is inserted. The nuclear fossa  
165 was located lateral, contributing to the asymmetry of the spermatozoa head.

166 The midpiece was attached to the posterior region of the nucleus and composed  
167 of the centrioles and mitochondria (Fig 3A,B). The mitochondria were small and round,  
168 each surrounded by an outer membrane that enveloped an inner membrane that  
169 surrounded the mitochondrial ridges (Fig 3B). The mitochondrial area was  $37.22 \pm 12.41$   
170  $\mu\text{m}^2$  in IS (Table 1). The plasma membrane of the midpiece formed a cytoplasmatic  
171 channel through which the flagellum passed (Fig 3A,C,D). It was a narrow and deep  
172 invagination that separates both structures.

173 The flagellum was composed of the axoneme surrounded by the plasma  
174 membrane. Specifically, the axoneme consisted of two central microtubules and nine  
175 pairs of peripheral microtubules ( $9 \times 2 + 2$ ) (Fig 3C,D). In addition, the presence of  
176 cytoplasmic vesicles was observed along the flagellum, which was an increase in the  
177 cytoplasm around the axoneme, causing protrusions and increasing the thickness of the  
178 flagellum (Fig 3A).

### 179 3.2. Morphological and ultrastructural changes in AS

180 SEM and TEM micrographs revealed that 60 seconds after motility activation, severe  
181 morphological and ultrastructural alterations occurred in the different regions of the  
182 zebrafish spermatozoa (Fig 4A-H). Altogether, metric data showed a significant increase  
183 (*t-test*;  $P < 0.001$ ) in the measurements of the different sperm structures after motility  
184 activation (Table 1).

185 Regarding sperm head, strong structural distortions were observed. SEM analysis  
 186 showed that AS exhibited a clear breakdown and disaggregation of the head compared to  
 187 IS (Fig 4A,B). Furthermore, TEM micrographs showed that the ultrastructure of the  
 188 nucleus in AS was altered since the characteristic spherical shape of the IS was replaced  
 189 by an asymmetric morphology (Fig 4C-H). Focusing on the genetic material, the AS  
 190 showed regions that were less electrically dense than in IS. Thus, head-related alterations  
 191 in AS included the swelling of the nucleus, the bursting of the plasma membrane, and the  
 192 decompression of the genetic material (Fig 4D,F,H). Morphological measurements also  
 193 corroborated these changes after activation since a significant increase (*t*-test;  $P < 0.001$ )  
 194 in head area and nucleus area was observed in AS compared to IS (Table 1).

195 Table 1.  
 196 Statistical data on morphology and ultrastructure of zebrafish sperm before and after motility  
 197 activation.

Parameter	Unit	IS		AS		<i>t</i>	<i>P</i> -value
		n	(mean ± SD)	n	(mean ± SD)		
Total length	μm	105	31.94 ± 2.01	-	-	-	-
Head length	μm	105	1.83 ± 0.12	100	2.18 ± 0.17	-16.338	<0.001
Head area	μm <sup>2</sup>	105	2.65 ± 0.36	100	3.74 ± 0.59	-15.817	<0.001
Nucleus length	μm	80	1.60 ± 0.14	80	2.07 ± 0.35	-11.031	<0.001
Nucleus area	μm <sup>2</sup>	80	2.03 ± 0.36	80	3.45 ± 1.12	-10.831	<0.001
Midpiece length	μm	100	0.59 ± 0.13	-	-	-	-
Midpiece width	μm	100	1.34 ± 0.19	-	-	-	-
Mitochondrial length	nm	50	181.58 ± 31.85	50	467.06 ± 91.27	-20.882	<0.001
Mitochondrial width	nm	50	256.02 ± 47.71	50	573.64 ± 113.72	-18.212	<0.001
Mitochondrial area	μm <sup>2</sup>	50	37.22 ± 12.41	50	212.09 ± 63.33	-19.158	<0.001
Flagellum length	μm	80	28.74 ± 2.14	-	-	-	-
Terminal piece length	μm	70	0.76 ± 0.14	-	-	-	-

198 Data are showed as number of measurements (n). Inactive sperm (IS); Active sperm (AS). *P*-value obtained  
 199 through unpaired two-sample *t*-test according to Levene's test for equality of variances (equal variances  
 200 assumed).

201

202 Otherwise, SEM micrographs revealed that the midpiece structure underwent a  
 203 sharp modification after activation (Fig 4A,B). Complementarily, the study of the  
 204 midpiece using TEM allowed characterizing the alterations in AS (Fig 4C-H).

205 Specifically, we detected the loss of the plasma membrane in the midpiece and a  
206 significant increase of mitochondrial area from IS to AS conditions (Table 1). Hence, the  
207 midpiece after activation was ultrastructurally affected since rupture of the plasma  
208 membrane and mitochondria alterations in morphology were observed (Fig 4D,F,H).

209 After motility activation, the morphology of the spermatozoa flagellum was also  
210 altered. SEM micrographs revealed that the vast majority of AS had coiled flagellum (Fig  
211 4A,B). The ultrastructural study by TEM also recorded cells with coiled flagellum around  
212 the head after motility activation (Fig 4D). Due to the morphological alterations that  
213 occurred after the activation of motility (as can be observed in Fig 4B), it was not  
214 possible to record by SEM the morphological measurements of the midpiece, the  
215 flagellum, and the total length of the spermatozoa.

#### 216 4. Discussion

217 Spermatozoa morphology and ultrastructure were studied in zebrafish before and after  
218 motility activation showing unexpected dramatic changes after activation. A detailed  
219 description of the spermatozoa morphology and ultrastructure provides useful data on fish  
220 phylogeny and taxonomy and favors the identification of relationships among  
221 spermatozoa phenetic characteristics and reproductive biology [19,22,23]. In addition,  
222 spermatozoa morphological and ultrastructural features are likely to be directly related to  
223 male fertility; and sperm exposed to different conditions may vary in their response  
224 through, for example, the interaction with endocrine disruptors or cryopreservation [24–  
225 26].

226 Sperm morphology has been studied in different species of teleost fish [6,23,27]  
227 and the spermatozoa ultrastructure of teleosts differs according to the taxonomic order.  
228 The shape of the nucleus is vastly variable and appears to be associated with the  
229 complexity of spermatogenesis [18]. Some spermatozoa, such as in salmonids, present

230 oval nuclei whereas others, such as in cyprinids, are spherical. The midpiece in teleosts  
231 is underdeveloped and consists of a central flagellum surrounded by a mitochondrial  
232 sheath [19]. Our TEM micrographs showed that the zebrafish sperm head was spherical,  
233 with some nuclear vesicles, and the NF was inserted asymmetrically. Moreover, the  
234 intermediate piece had a very characteristic morphology since it formed a highly  
235 pronounced cytoplasmatic channel. Finally, the flagellum consisted of a single long thin  
236 cylinder that protrudes from the spermatozoa head. Overall, our ultrastructural results  
237 from IS condition confirmed previous observations [28].

238         It is worth noting that the activation of fish spermatozoa by contact with water is  
239 crucial for reproductive biology because during the brief motility duration, activated  
240 spermatozoa must be able to reach, bind, penetrate eggs, and initiate fertilization [16,17].  
241 Additionally, motility activation in fish sperm is essential for the evaluation of  
242 spermatozoa quality for induced spawning, development of spermatozoa  
243 cryopreservation protocols, and research activities that involve spermatozoa competition  
244 [29]. In this study, we performed a comprehensive analysis of the ultrastructure 60  
245 seconds after motility activation with tap water in zebrafish spermatozoa.

246         Notably, we found considerable DNA damage using SEM and TEM in zebrafish  
247 AS. Particularly, TEM micrographs showed a marked decondensation of the genetic  
248 material as shown by less electron-dense regions in the nucleus after motility activation.  
249 Additionally, we observed strong morphological distortions of the head as a result of  
250 swelling of the nucleus and the bursting of the plasma membrane. These modifications  
251 were also detected by metric analysis where significant increases were recorded in all  
252 sperm measurements after motility activation. The integrity of the sperm DNA is crucial  
253 for the proper development and fitness of future generations. The damage in the DNA of  
254 zebrafish spermatozoa after activation has been described previously using other

255 techniques such as Sperm Chromatin Dispersion (SCD) test, *In situ* nick translation  
256 (ISNT), DNA Breakage Detection-Fluorescence In Situ Hybridization (DBD-FISH), and  
257 Comet assay [30]. Furthermore, another study using TUNEL assay  
258 (Terminal deoxynucleotidyl transferase dUTP Nick-End Labeling) revealed that the  
259 percentage of spermatozoa with DNA fragmentation increases as the motility activation  
260 time increases and more so in the presence of a rival male suggesting that this may have  
261 negative effects on sperm quality [20]. DNA damage may be due to the low compaction  
262 of the genetic material, since the transition to protamines does not occur in the  
263 spermatozoa of the zebrafish [31].

264 Mitochondria are the energy supplier that allows flagellar movement and possess  
265 a fundamental role for fish spermatozoa motility, integrity, and fertilizing potential [18].  
266 In different marine teleost species, black porgy (*Acanthopagrus schlegelli*), black grouper  
267 (*Epinephelus malabaricus*), and Atlantic croaker (*Micropogonias undulatus*), size and  
268 number of mitochondria decrease and eventually disappear after spermatozoa activation  
269 with artificial sea water [12]. However, in zebrafish, our observations differ somewhat  
270 with previous findings since we recorded a significant increase of the mitochondrial area  
271 in AS compared to IS. Therefore, the visualization of mitochondria by means of TEM is  
272 essential to know how mitochondrial dysfunctions could have a direct effect on structural  
273 and functional damage to the spermatozoa. Moreover, our TEM micrographs revealed  
274 that zebrafish spermatozoa midpiece was deeply affected, with the rupture of the cell  
275 membrane.

276 Proper spermatozoa flagellar motility, functionality, and ultrastructure is essential  
277 to reach the oocyte and fertilize it [16,17]. In this context, our results revealed that, after  
278 motility activation, a high percentage of spermatozoa showed a coiled flagellum and a  
279 disaggregated flagellar plasma membrane. However, the severe morphological

280 deformations that occurred in the sperm after activation prevented the detailed recording  
281 of the measurements of the midpiece and the flagellum. Our data complement a previous  
282 report in which we recorded the percentage of zebrafish spermatozoa with coiled  
283 flagellum after different times of motility activation and subjected to different levels of  
284 spermatozoa competition [20]. Similarly, the swelling in spermatozoa head and a  
285 progressive but reversible coiling of the flagellum was observed after short-term exposure  
286 to freshwater in the carp (*Cyprinus carpio*) [14]. Morphological changes because of  
287 osmolarity have also been described in the northern pike flagellum (*Esox lucius*) [6].

## 288 5. Conclusions

289 In summary, dramatic morphological and ultrastructural damage occurs in zebrafish  
290 spermatozoa after motility activation. These alterations associated with hypoosmotic  
291 shock seem to be the main cause of the short activation time of zebrafish spermatozoa.  
292 Overall, motility activation leads to substantial ultrastructural alterations of the zebrafish  
293 spermatozoa, possibly modifying the physiology and decreasing the reproductive  
294 potential.

## 295 Acknowledgments

296 This research was funded by the Human Fertility Cathedra of the University of Alicante  
297 and the VIGROB-186.

## 298 Competing interests

299 The authors declare that they have no conflict of interest.

## 300 Data statement

301 All data generated or analyzed during this study are included in this published article and  
302 it is uploaded in a database repository.

303

304 **Author contribution**

305 **Paula Sáez-Espinosa**: Methodology, Investigation, Formal analysis, Writing e review &  
306 editing. **Cristina Franco-Esclapez**: Investigation, Writing e review & editing. **Willian**  
307 **T. A. F. Silva**: Investigation, Text review & editing. **Alejandro Romero**: Investigation,  
308 Data curation, Text review & editing. **Simone Immler**: Conceptualization, Supervision,  
309 Text review & editing. **María José Gómez-Torres**: Conceptualization, Methodology,  
310 Supervision, Project administration, Funding acquisition, Text review & editing.

311 **References**

- 312 [1] Leal MC, Cardoso ER, Nobrega RH, Batlouni SR, Bogerd J, Franca LR, et al.  
313 Histological and stereological evaluation of zebrafish (*Danio rerio*)  
314 spermatogenesis with an emphasis on spermatogonial generations. *Biol Reprod*  
315 2009;81:177–87. <https://doi.org/10.1095/biolreprod.109.076299> [doi].
- 316 [2] Teame T, Zhang Z, Ran C, Zhang H, Yang Y, Ding Q, et al. The use of zebrafish  
317 (*Danio rerio*) as biomedical models. *Anim Front Rev Mag Anim Agric*  
318 2019;9:68–77. <https://doi.org/10.1093/af/vfz020> [doi].
- 319 [3] Hoo JY, Kumari Y, Shaikh MF, Hue SM, Goh BH. Zebrafish: A Versatile  
320 Animal Model for Fertility Research. *Biomed Res Int* 2016;2016:9732780.  
321 <https://doi.org/10.1155/2016/9732780> [doi].
- 322 [4] Akhter A, Kumagai R, Roy SR, Ii S, Tokumoto M, Hossain B, et al. Generation  
323 of Transparent Zebrafish with Fluorescent Ovaries: A Living Visible Model for  
324 Reproductive Biology. *Zebrafish* 2016;13:155–60.  
325 <https://doi.org/10.1089/zeb.2015.1116> [doi].
- 326 [5] He JH, Gao JM, Huang CJ, Li CQ. Zebrafish models for assessing developmental  
327 and reproductive toxicity. *Neurotoxicol Teratol* 2014;42:35–42.  
328 <https://doi.org/10.1016/j.ntt.2014.01.006> [doi].

- 329 [6] Alavi SM, Rodina M, Viveiros AT, Cosson J, Gela D, Boryshpolets S, et al.  
330 Effects of osmolality on sperm morphology, motility and flagellar wave  
331 parameters in Northern pike (*Esox lucius* L.). *Theriogenology* 2009;72:32–43.  
332 <https://doi.org/10.1016/j.theriogenology.2009.01.015> [doi].
- 333 [7] Cosson J. The Ionic and Osmotic Factors Controlling Motility of Fish  
334 Spermatozoa. *Aquac Int* 2004;12:69–85.  
335 <https://doi.org/10.1023/B:AQUI.0000017189.44263.bc>.
- 336 [8] Domínguez-Castanedo O, Toledano-Olivares Á, Martínez-Espinosa D, Ávalos-  
337 Rodríguez A. Cambios morfológicos en gametos del barbo tigre *Puntius*  
338 *tetrazona* (Cypriniformes: Cyprinidae) e implementación de la fertilización in  
339 vitro. *Rev Biol Trop* 2014;62:1353–63.
- 340 [9] Tabares C, Morales A, Olivera-Angel M. Fisiología de la activación del  
341 espermatozoide en peces de agua dulce. *Rev Colomb Ciencias Pecu ISSN 0120-*  
342 *0690, Vol 18, N° 2, 2005, Pags 149-161 2005;18.*
- 343 [10] Fechner S, Alvarez L, Bönigk W, Müller A, Berger TK, Pascal R, et al. A K(+)-  
344 selective CNG channel orchestrates Ca(2+) signalling in zebrafish sperm. *Elife*  
345 2015;4. <https://doi.org/10.7554/eLife.07624>.
- 346 [11] Jing R, Huang C, Bai C, Tanguay R, Dong Q. Optimization of activation,  
347 collection, dilution, and storage methods for zebrafish sperm. *Aquaculture*  
348 2009;290:165—171. <https://doi.org/10.1016/j.aquaculture.2009.02.027>.
- 349 [12] Gwo JC. Ultrastructural study of osmolality effect on spermatozoa of three  
350 marine teleosts. *Tissue Cell* 1995;27:491–7. [https://doi.org/S0040-](https://doi.org/S0040-8166(05)80057-6)  
351 [8166\(05\)80057-6](https://doi.org/S0040-8166(05)80057-6) [pii].
- 352 [13] Dreanno C, Cosson J, Suquet M, Cibert C, Fauvel C, Dorange G, et al. Effects of  
353 osmolality, morphology perturbations and intracellular nucleotide content during

- 354 the movement of sea bass (*Dicentrarchus labrax*) spermatozoa. *J Reprod Fertil*  
355 1999;116:113–25. <https://doi.org/10.1530/jrf.0.1160113> [doi].
- 356 [14] Perchec G, Cosson MP, Cosson J, Jeulin C, Billard R. Morphological and kinetic  
357 changes of carp (*Cyprinus carpio*) spermatozoa after initiation of motility in  
358 distilled water. *Cell Motil* 1996;35:113–20.  
359 [https://doi.org/https://doi.org/10.1002/\(SICI\)1097-0169\(1996\)35:2<113::AID-](https://doi.org/https://doi.org/10.1002/(SICI)1097-0169(1996)35:2<113::AID-CM4>3.0.CO;2-B)  
360 [CM4>3.0.CO;2-B](https://doi.org/https://doi.org/10.1002/(SICI)1097-0169(1996)35:2<113::AID-CM4>3.0.CO;2-B).
- 361 [15] Coward K, Bromage NR, Hibbitt O, Parrington J. Gamete physiology,  
362 fertilization and egg activation in teleost fish. *Rev Fish Biol Fish* 2002;12:33–58.  
363 <https://doi.org/10.1023/A:1022613404123>.
- 364 [16] Sadeghi S, Nunez J, Soler C, Silvestre M. Effect of the activation media with  
365 different osmolality and cool storage on spermatozoa motility parameters over  
366 time in zebrafish, *Danio rerio*. *Turkish J Fish Aquat Sci* 2017;17:111–20.  
367 [https://doi.org/10.4194/1303-2712-v17\\_1\\_13](https://doi.org/10.4194/1303-2712-v17_1_13).
- 368 [17] Wilson-Leedy JG, Kanuga MK, Ingermann RL. Influence of osmolality and ions  
369 on the activation and characteristics of zebrafish sperm motility. *Theriogenology*  
370 2009;71:1054–62. <https://doi.org/10.1016/j.theriogenology.2008.11.006> [doi].
- 371 [18] Ulloa-Rodriguez P, Figueroa E, Diaz R, Lee-Estevez M, Short S, Farias JG.  
372 Mitochondria in teleost spermatozoa. *Mitochondrion* 2017;34:49–55.  
373 [https://doi.org/S1567-7249\(17\)30004-1](https://doi.org/S1567-7249(17)30004-1) [pii].
- 374 [19] Lahnsteiner F, Patzner RA. Sperm morphology and ultrastructure in fish, 2008.
- 375 [20] Silva WTAF, Saez-Espinosa P, Torijo-Boix S, Romero A, Devaux C, Durieux M,  
376 et al. The effects of male social environment on sperm phenotype and genome  
377 integrity. *J Evol Biol* 2019;32:535–44. <https://doi.org/10.1111/jeb.13435> [doi].
- 378 [21] Westerfield M. The zebrafish book : a guide for the laboratory use of zebrafish

- 379 (Danio rerio). 5th Editio. Eugene, OR: Printed by the University of Oregon Press;  
380 2007.
- 381 [22] Haszprunar G, Jamieson, B. G. M. 1991. Fish Evolution and Systematics:  
382 Evidence from Spermatozoa. With a survey of lophophorate, echinoderm and  
383 protochordate sperm and an account of gamete cryopreservation. Cambridge  
384 University Press, Cambridge. xiv + 319 pp. ISBN 0-52. J Evol Biol 1992;5:721–  
385 3. <https://doi.org/https://doi.org/10.1046/j.1420-9101.1992.5040721.x>.
- 386 [23] Psenicka M, Rodina M, Nebesarova J, Linhart O. Ultrastructure of spermatozoa  
387 of tench *Tinca tinca* observed by means of scanning and transmission electron  
388 microscopy. Theriogenology 2006;66:1355–63. [https://doi.org/S0093-](https://doi.org/S0093-691X(06)00276-7)  
389 [691X\(06\)00276-7](https://doi.org/S0093-691X(06)00276-7) [pii].
- 390 [24] Billard R, Cosson J, Linhart O. Changes in the flagellum morphology of intact  
391 and frozen/thawed Siberian sturgeon *Acipenser baeri* Brandt sperm motility.  
392 Aquac Res 2001;31:283–7. <https://doi.org/10.1046/j.1365-2109.2000.00423.x>.
- 393 [25] Butts IAE, Rideout RM, Burt K, Samuelson S, Lush L, Litvak MK, et al.  
394 Quantitative semen parameters of Atlantic cod (*Gadus morhua*) and their  
395 physiological relationships with sperm activity and morphology. J Appl Ichthyol  
396 2010;26:756–62. [https://doi.org/https://doi.org/10.1111/j.1439-](https://doi.org/https://doi.org/10.1111/j.1439-0426.2010.01545.x)  
397 [0426.2010.01545.x](https://doi.org/https://doi.org/10.1111/j.1439-0426.2010.01545.x).
- 398 [26] Hatef A, Alavi SMH, Butts IAE, Policar T, Linhart O. Mechanism of action of  
399 mercury on sperm morphology, adenosine triphosphate content, and motility in  
400 *Perca fluviatilis* (Percidae; Teleostei). Environ Toxicol Chem 2011;30:905–14.  
401 <https://doi.org/10.1002/etc.461>.
- 402 [27] Neznanova SY. Comparative analysis of gamete ultrastructure in big-scaled  
403 redbfin *Tribolodon hakonensis* (Cyprinidae) from Southern Primorye and

- 404 Sakhalin. *J Ichthyol* 2015;55:900–5.
- 405 <https://doi.org/10.1134/S0032945215050100>.
- 406 [28] Zhang L, Wang S, Chen W, Hu B, Ullah S, Zhang Q, et al. Fine Structure of  
407 Zebrafish (*Danio rerio*) Spermatozoa. *Pak Vet J* 2013;ISSN:253–8318.
- 408 [29] Dzyuba V, Cosson J. Motility of fish spermatozoa: from external signaling to  
409 flagella response. *Reprod Biol* 2014;14:165–75.
- 410 <https://doi.org/10.1016/j.repbio.2013.12.005> [doi].
- 411 [30] Gosálvez J, López-Fernández C, Hermoso A, Fernández JL, Kjelland ME. Sperm  
412 DNA fragmentation in zebrafish (*Danio rerio*) and its impact on fertility and  
413 embryo viability — Implications for fisheries and aquaculture. *Aquaculture*  
414 2014;433:173–82.
- 415 <https://doi.org/https://doi.org/10.1016/j.aquaculture.2014.05.036>.
- 416 [31] Wu SF, Zhang H, Cairns BR. Genes for embryo development are packaged in  
417 blocks of multivalent chromatin in zebrafish sperm. *Genome Res* 2011;21:578–  
418 89. <https://doi.org/10.1101/gr.113167.110> [doi].
- 419

420 **Figure captions**

421

422 **Fig 1.** Experimental design followed in this study. (A) experimental conditions:  
 423 inactivated spermatozoa (IS) and activated spermatozoa (AS) 60 seconds after activation.  
 424 (B) Spermatozoa morphology and ultrastructure was observed by using Scanning  
 425 Electron Microscopy (SEM) and Transmission Electron Microscopy (TEM),  
 426 respectively.

427

428 **Fig 2.** SEM micrographs showing the morphology of zebrafish inactivated (IS)  
 429 spermatozoa. (A) General view of zebrafish spermatozoa morphology. (B) Detailed  
 430 aspect of the spermatozoa head and midpiece. Head (H); midpiece (MP); flagellum (F);  
 431 terminal piece (TP).

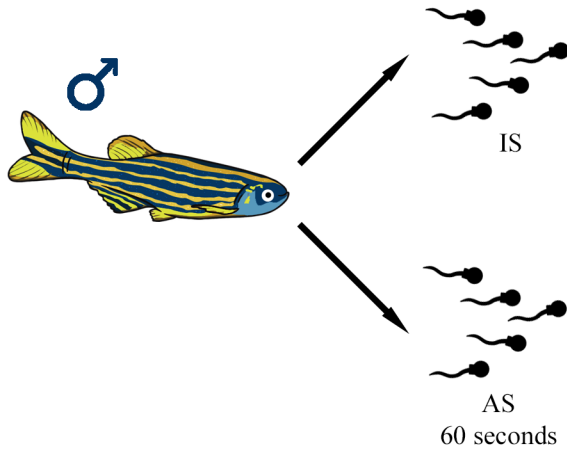
432

433 **Fig 3.** TEM micrographs showing the ultrastructure of zebrafish inactivated (IS)  
 434 spermatozoa. (A) longitudinal section of head, midpiece, and flagellum. (B) Detailed  
 435 longitudinal section of mitochondria located in midpiece. (C) Detailed transversal section  
 436 of axoneme. (D) Longitudinal section of head, midpiece, and axoneme. (E) Longitudinal  
 437 section of head with nuclear vesicles. (F) Schematic organization of zebrafish  
 438 spermatozoa ultrastructure. Head (H); midpiece (MP); flagellum (F); nucleus (N);  
 439 proximal centriole (PC); distal centriole (DC); nuclear fossa (NF); cytoplasmic channel  
 440 (CC); cytoplasmic vesicles (CV); mitochondria (Mi); mitochondria external membrane  
 441 (MiEM); mitochondria internal membrane (MiIM); axoneme (A); dynein arm (DA);  
 442 nuclear membrane (NM); plasma membrane (PM); nuclear vesicles (NV).

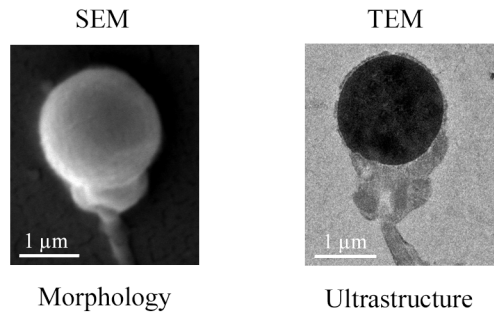
443

444 **Fig 4.** Morphological and ultrastructural comparison of zebrafish inactivated spermatozoa  
 445 (IS) and activated spermatozoa (AS). (A) SEM micrograph of IS. (B) SEM micrograph  
 446 of AS. (C,E,G) TEM micrographs showing the ultrastructure of IS. (D,F,H) TEM  
 447 micrographs showing the ultrastructure of AS. Head (H); midpiece (MP); flagellum (F);  
 448 coiled flagellum (CF); nucleus (N); cytoplasmic channel (CC); mitochondria (Mi);  
 449 nuclear fossa (NF); nuclear membrane (NM); Plasma membrane (PM); Scanning Electron  
 450 Microscopy (SEM); Transmission Electron microscopy (TEM). Note the severe  
 451 ultrastructural damage after the motility activation.

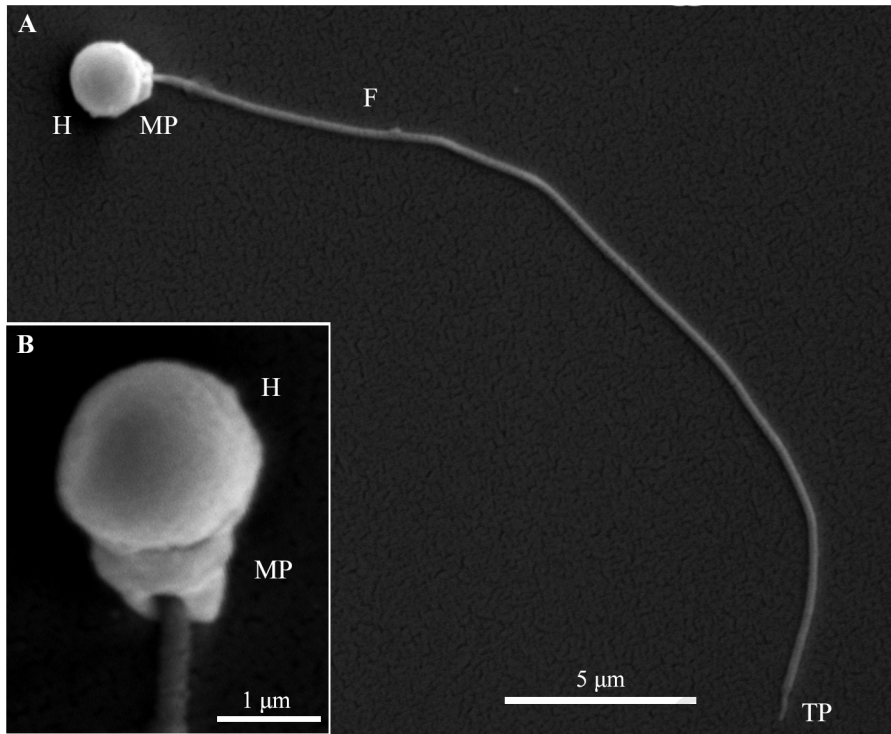
A

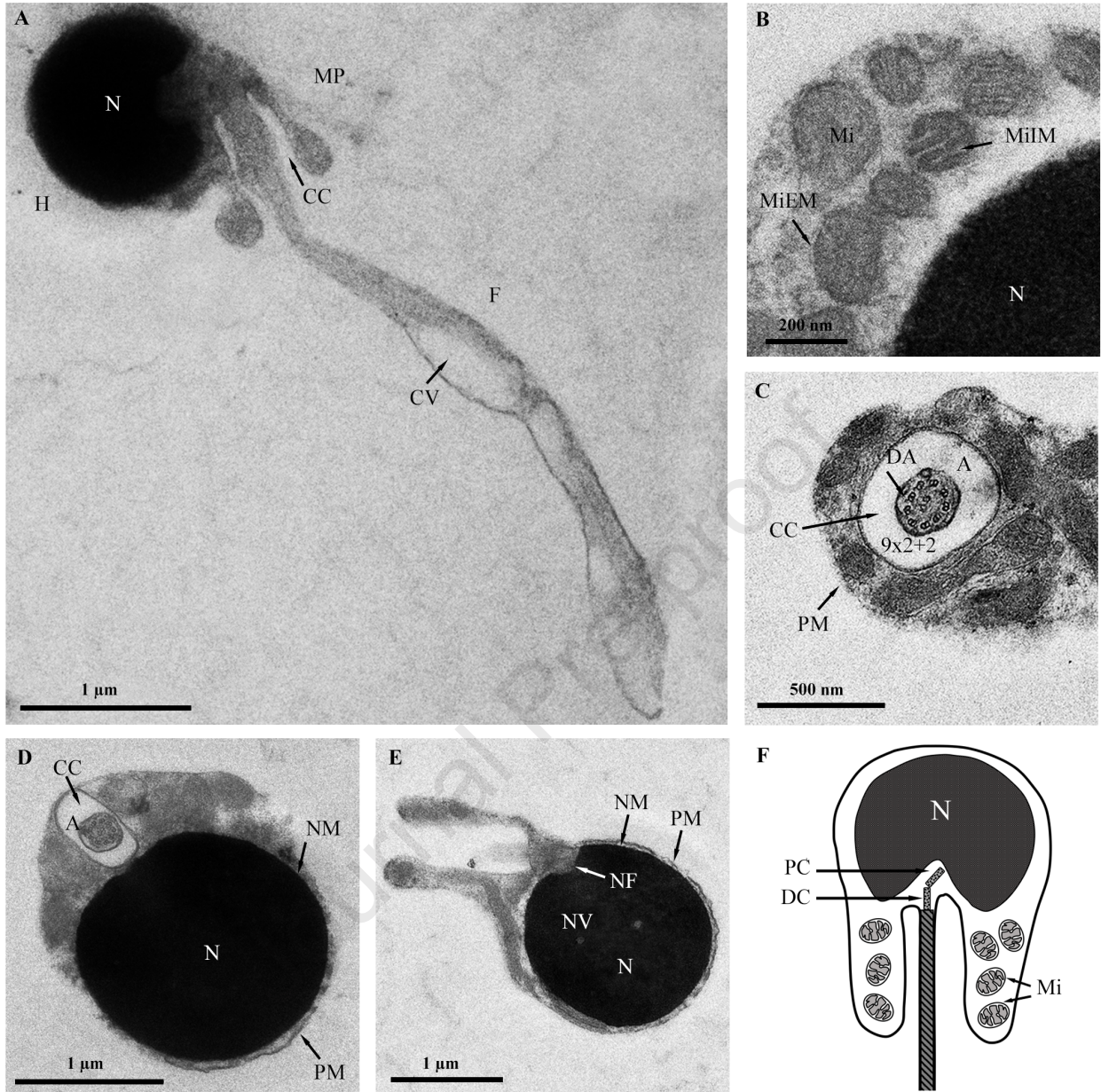


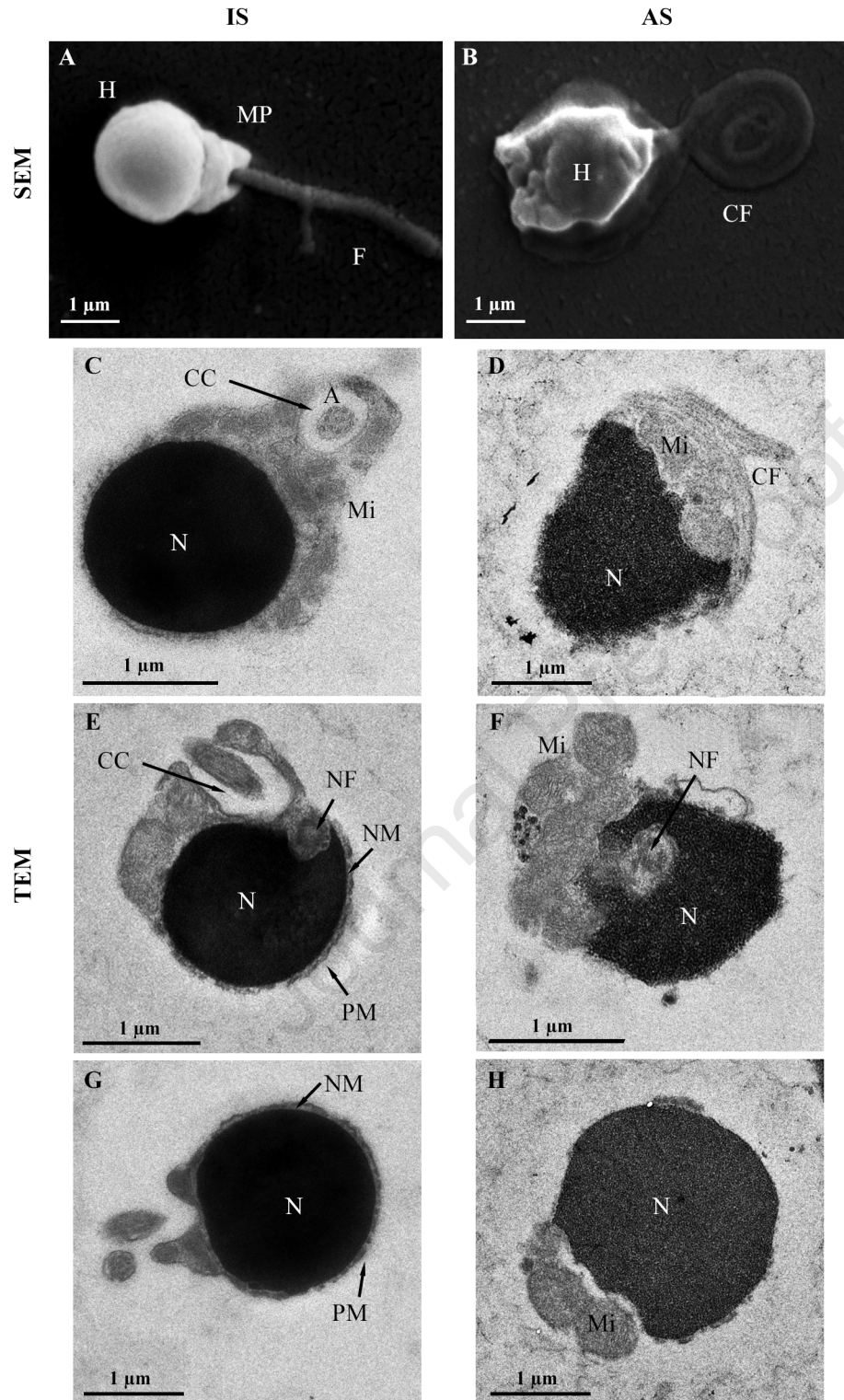
B



Journal Pre-proof







## Highlights

- Zebrafish spermatozoa activation leads to substantial ultrastructural changes.
- TEM micrographs show a marked DNA decondensation after activation.
- After activation, many sperm have a coiled flagellum and a disaggregated membrane.

Journal Pre-proof